Tuning of chaotic surface spin waves in a magnetic-film feedback ring via the ring gain

Aaron Hagerstrom,[1] Mingzhong Wu,[1,*] Richard Eykholt,[1] and Boris A. Kalinikos[2]
[1]*Department of Physics, Colorado State University, Fort Collins, Colorado 80523, USA*
[2]*St. Petersburg Electrotechnical University, 197376 St. Petersburg, Russia*
(Received 13 September 2010; published 9 March 2011)

This paper reports on experimental data on the controlled tuning of chaotic surface spin waves in a magnetic-film active feedback ring. The chaotic behavior of these waves arises through three-wave nonlinear interactions. With a change in the ring gain, two chaotic regimes were observed. One corresponds to the situation where only one ring eigenmode was excited in the ring, while the other corresponds to the situation where two ring eigenmodes were excited. The correlation dimension and autocorrelation function (ACF) properties of the chaotic wave in each regime strongly depend on the level of the ring gain, and this gain dependence differs from one regime to the other. The shift between the two regimes was not a smooth transition. In particular, one observed a sharp change in both the correlation dimension and the distance of the side ACF peaks to the main ACF peak.

DOI: 10.1103/PhysRevB.83.104402 PACS number(s): 75.30.Ds, 05.45.−a, 76.50.+g, 85.70.Ge

I. INTRODUCTION

If one amplifies the output signal from a dissipative transmission line and then feeds it back to the input of the transmission line, one forms an active feedback ring system. Such a ring system represents a driven damped system. Specifically, the energy loss of the wave that propagates in the transmission line is compensated by the energy gain provided by the amplifier. Examples of this type of feedback ring include electromagnetic transmission line oscillators,[1–3] magnetic thin-film feedback rings,[4–7] and fiber ring lasers,[8–12] among others. These systems have proved to be very useful for fundamental studies of nonlinear dynamics.

There are two main focus areas in the study of nonlinear waves in active feedback rings, (i) envelope solitons and (ii) chaos. Previous experiments have demonstrated envelope solitons in a wide variety of ring configurations.[1,5,7,10,11] There are two fine balances that are involved in the formation of these solitons, (i) a balance between the dispersion-induced self-broadening and the nonlinearity-induced self–narrowing, and (ii) a balance between the internal energy loss and the energy gained from external sources. Note that conventional solitons in conservative systems involve only the first balance, not the second.[13] In this sense, the solitons in active feedback rings are fundamentally different from conventional solitons and are called "dissipative solitons."[14] Dissipative solitons can exist in different forms including, for example, stationary solitons, pulsating solitons, or exploding solitons.[10,14,15]

Chaos in active feedback rings has been demonstrated both experimentally and theoretically. The main focus of previous experiments has been on the use of different configurations to demonstrate chaotic excitations through different nonlinear processes.[2–4,6,8,10,11] Theoretical study has been focused on new models for chaotic excitations in certain ring systems, the roles of different physical processes in chaotic excitations, and the transition to chaos through changing various control parameters, such as the ring gain coefficient.[8–12]

This paper reports the controlled tuning of chaos complexity by the ring gain for chaotic spin waves in a magnetic thin-film active feedback ring. With a change in ring gain, two different chaotic regimes were observed. One corresponds to the situation where only one ring eigenmode was excited in the ring, while the other corresponds to the situation where two ring eigenmodes were excited. It was demonstrated that one could make use of the ring gain to effectively control both the chaotic behavior in each regime and the transition between the two regimes.

The main results are as follows. (i) In the one-eigenmode regime, as one increases the ring gain, the correlation dimension increases roughly linearly, the main peak in the autocorrelation function (ACF) profile becomes narrower, and the side peaks in the ACF profile move towards the main peak and, at the same time, become weaker. (ii) At a certain ring gain level, one observes a shift from the one-eigenmode regime to the two-eigenmode regime. This shift is not a smooth transition. In particular, one observes a jump in both the correlation dimension and the distance of the side ACF peaks to the main ACF peak. (iii) In the two-eigenmode regime, with an increase in ring gain, the correlation dimension still increases, but at a greater rate, and the ACF side peaks still move towards the main peak, but at a slower rate. The amplitudes of the side peaks show a response opposite to that in the one-eigenmode regime—they increase with ring gain. The change of the main peak width with gain, however, is similar to that in the one-eigenmode regime.

These results show rich complexity for chaotic spin waves in magnetic-film feedback rings. Such complexity has not been demonstrated in previous works.[4,6,16–20] It is also important to emphasize that the chaos in those previous works involved the excitation of many ring eigenmodes. In contrast, the chaos in this work involved the excitation of only one or two eigenmodes. In addition, it is also important to highlight that this work demonstrates a new tunable microwave chaotic oscillator. Oscillators where the features of chaos can be tuned easily are critically needed by high-resolution chaotic radars,[21,22] radars for complex target detection,[23,24] and microwave chaotic communications.[25]

II. EXPERIMENT

The experimental arrangement is shown in Fig. 1. The feedback ring consisted of a magnetic yttrium iron garnet (YIG) thin-film strip and two microstrip line transducers

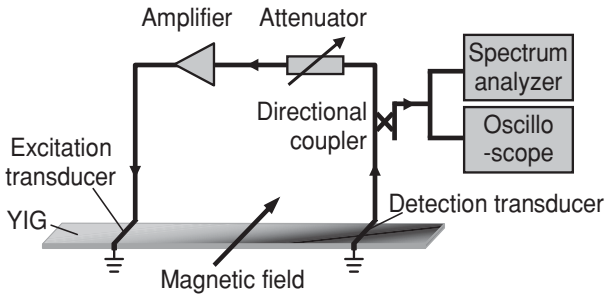

FIG. 1. Schematic of experimental setup.

placed over the YIG strip to excite and detect spin waves. The output signal from the detection transducer was fed back to the excitation transducer through a broadband microwave amplifier and a tunable microwave attenuator. The YIG strip was magnetized to saturation by a static magnetic field which was in the plane of the YIG film strip and perpendicular to the length of the strip. This film-field configuration supports the propagation of surface spin waves along the film strip.[26,27] The magnetic field was set to be relatively low so that the three-wave parametric interactions between the surface and backward volume spin waves were allowed.[28] It was these three-wave processes that drove the excitation of chaos in the ring. The ring signal was sampled through a directional coupler, with feeds to a spectrum analyzer for frequency analysis and a broadband fast oscilloscope for temporal signal measurements.

For the data presented below, the YIG strip was 5.0 μm thick, 1.3 mm wide, and 22.2 mm long. It was cut from a larger single-crystal YIG film grown on a gadolinium gallium garnet substrate by liquid phase epitaxy. The YIG film had unpinned surface spins. The magnetic field was 85 Oe. The microstrip line transducers were 50-μm-wide and 2-mm-long elements. The transducer separation was held at about 4.4 mm. The microwave amplifier was tunable through a dc bias voltage. It had a maximum output power of 3 W and a linear response over a frequency range of 0.4–3.0 GHz. These characteristics ensured that the nonlinear response of the feedback ring was determined by the YIG film only.

III. RESULTS AND DISCUSSION

The feedback ring can have a number of resonance eigenmodes that exhibit low decay rates.[7] The frequencies of these eigenmodes can be determined by the phase condition $k(\omega)l + \phi_e = 2\pi n$, where k is the spin-wave wave number, ω is the spin-wave frequency, l is the transducer separation, ϕ_e is the phase shift introduced by the electronic circuits, and n is an integer. At a low ring gain G, all of the eigenmodes experience an overall net loss and there is no spontaneous signal in the ring. If the ring gain is increased to a certain threshold level, here taken as $G = 0$, the eigenmode with the lowest decay rate will start to self-generate in the ring and one will obtain a continuous-wave response at this eigenmode frequency. A further increase in gain leads to the excitation of sideband modes and the broadening of the power spectrum through three-wave processes as well as the generation of a second ring eigenmode, as reported below.

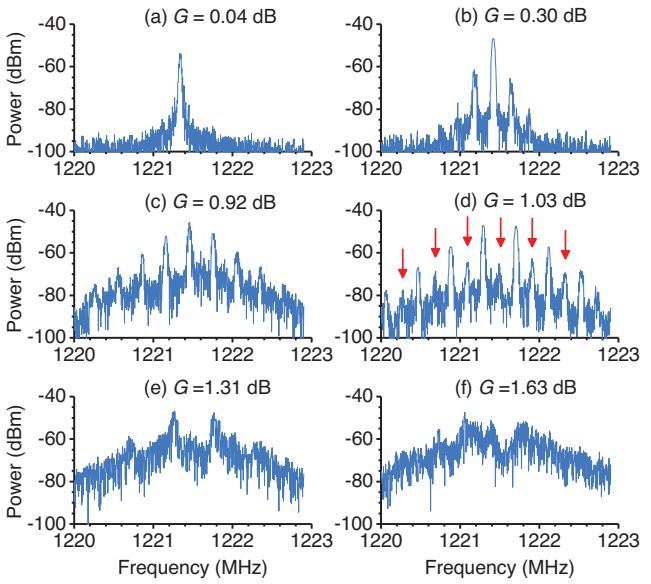

FIG. 2. (Color online) Power-frequency spectra for ring signals obtained at different ring gain G, as indicated.

Figure 2 shows representative power-frequency spectra for ring signals obtained at different ring gains, as indicated. As shown in graph (a), the spectrum obtained for a ring gain slightly higher than zero consists of a single peak. This peak corresponds to the ring eigenmode with the lowest decay rate. When the gain was increased to 0.30 dB, as shown in graph (b), the initial mode became stronger and several side modes were generated. These side modes were not ring eigenmodes. Rather, they were new modes excited through the three-wave processes. As discussed below, other ring eigenmodes were indeed far away from the frequency range shown in Fig. 1. As the gain was increased further, one observed the excitation of more side modes, as shown in graph (c), and then an increase in the frequency spacing of the modes and a frequency halving (period doubling) effect, as shown in graph (d). Note that, in (d), the new peaks showing the frequency halving are identified by vertical arrows. A further increase in ring gain leads to the washout of the modes and the realization of chaotic spectra, as shown in graphs (e) and (f).

As the gain was increased to 1.63 dB, for which the spectrum is shown in Fig. 1(f), a new peak appeared at a frequency which was about 30 MHz lower than the frequency of the first eigenmode discussed above. This new mode is a ring eigenmode. Figure 3 shows the spectra for this second eigenmode. As shown in graph (a), this mode is very weak at $G = 1.63$ dB. With an increase in G, one sees the enhancement of this mode as shown in graph (b), the excitation of new side modes as shown in graph (c), and then the washout of the modes as shown in graph (d). Note that, for the gain levels discussed here, the entire spectrum consists of both the first and second ring eigenmodes. Figure 3 shows only a portion of the entire spectrum near the second eigenmode. The portion for the first ring eigenmode is similar to the one shown in Fig. 2(f) and is not shown in Fig. 3.

The data in the time domain conform to the responses described above. Figure 4 shows representative time-domain

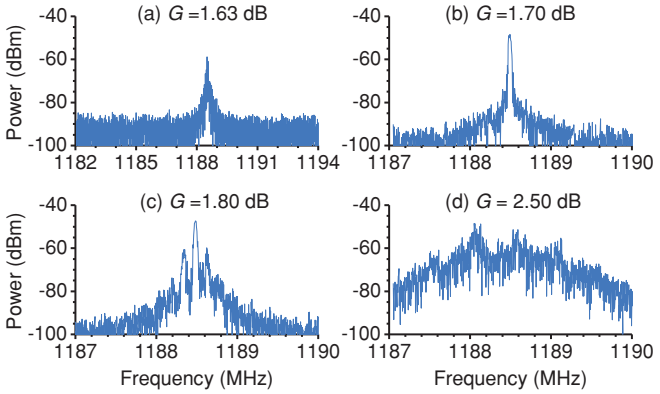

FIG. 3. (Color online) Power-frequency spectra for ring signals obtained at different ring gain G, as indicated.

signals—the envelopes of the signals in a power vs. time format. Graph (a) shows a train of pulses that is almost periodic. This signal corresponds to the almost uniform frequency comb shown in Fig. 2(c). Note that the period of this signal is two orders of magnitude longer than the ring round-trip time. The data in graph (b) for $G = 1.03$ dB show a train of pulses whose period doubles that shown in graph (a). This period doubling agrees with the frequency halving shown in Fig. 2(d) for the same gain level. At $G = 1.63$ dB, as shown in graph (c), one sees chaotic behavior in both the pulse amplitude and the pulse separation. This behavior corresponds to the chaotic spectrum shown in Fig. 2(f). The signal shown in graph (d) is also chaotic, just like the one shown in graph (c). If one increases the time scale by a factor of 10, however, one can see fast oscillations in the signal envelope. Such oscillations result from the beating of the two eigenmodes.

The frequency- and time-domain data presented above clearly show the development of chaotic spin waves in the feedback ring. These data, however, provide no direct information on the complexity of the chaotic signals. In order to obtain an insight into the chaos complexity, the correlation dimensions and autocorrelation functions of the obtained chaotic signals were computed.

Correlation dimension is the mostly widely used fractal dimension for chaos characterization.[29,30] The computation of the correlation dimensions involves four main steps.

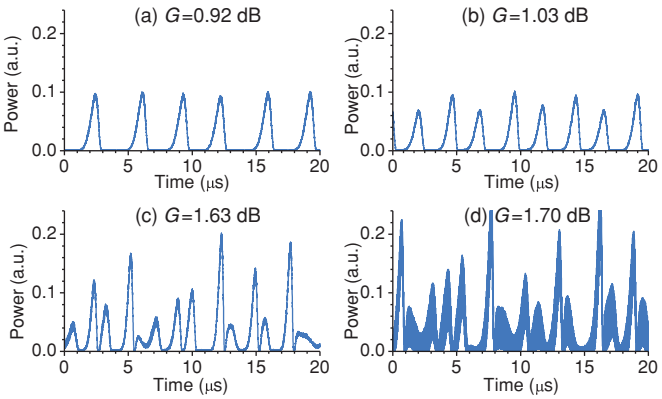

FIG. 4. (Color online) Time-domain signals obtained at different ring gain G, as indicated.

(i) Construction of an m-dimensional attractor from the time-domain data $V(t_i)$ through the method of time delays with a fixed delay window. The coordinates of the attractor were constructed as follows:

$$X_i = \{V(t_i),\ V(t_i + \tau), V(t_i + 2\tau), \ldots, V[t_i + (m-1)\tau]\}, \tag{1}$$

where τ is the time delay and m is the embedding dimension. The time delay τ varies with the embedding dimension m according to $\tau = \tau_w/(m-1)$, where τ_w is the fixed time delay window. For the calculation in this work, the delay window τ_w was determined by the use of a correlation integral approach[31] and was around 2.5 μs. (ii) Calculation of the fraction of the pairs of points on the attractor whose sup-norm separation is no greater than a probing distance r. This fraction is called the correlation sum C. (iii) Calculation of the correlation sum C for many different probing distances r. This allows for the plotting of $\log_{10}(C)$ vs. $\log_{10}(r)$, and the resultant plot is called the correlation plot. (iv) Determination of the slope of the correlation plot. The correlation sum C scales with the probing distance r according to a power law of the form

$$C(r) \propto r^D, \tag{2}$$

where the exponent D is the so-called correlation dimension. For this reason, the slope of the $\log_{10}(C)$ vs. $\log_{10}(r)$ plot is the correlation dimension D. When one increases the embedding dimension of an attractor, the correlation dimension increases initially and then reaches a limit when the embedding space is large enough for the attractor to untangle itself. This limiting correlation dimension is the fractal dimension of the chaotic signal $V(t_i)$.

Figure 5 shows representative data on the correlation dimensions. Graphs (a), (b), and (c) show a three-dimensional attractor, correlation plots for embedding dimension $m = 2$–35, and the D vs. m response, respectively, for the signal obtained at $G = 1.31$ dB. Graph (d) shows the dimension as a function of ring gain. The circles show the data, and the lines show the linear fits.

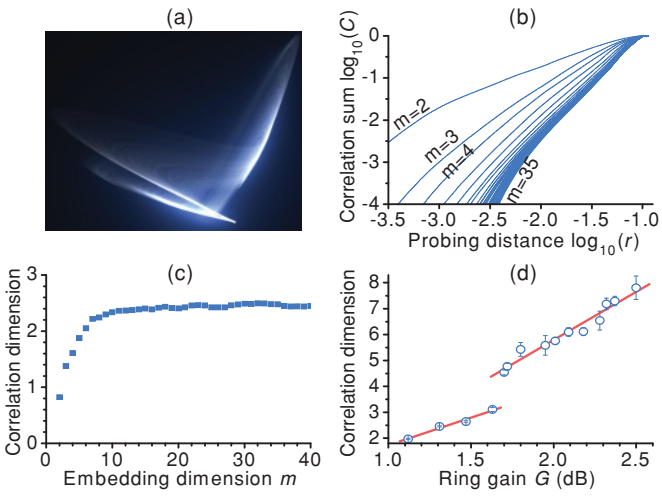

FIG. 5. (Color online) Chaotic characterization of ring signals. (a) 3D attractor. (b) Correlation plots. (c) Correlation dimension vs. embedding dimension. (d) Correlation dimension as a function of ring gain. The data in (a)–(c) are for the $G = 1.31$ dB signal.

The attractor in graph (a) is smooth and has a visible structure. The correlation plots in graph (b) all show a linear regime, and the slopes of the plots in these regimes yield the correlation dimension data shown in graph (c). The response in graph (c) shows rather clearly saturation behavior and indicates a fractal dimension of about 2.45. These results clearly indicate the chaotic nature of the measured signal.

The data in Fig. 5(d) show four things. (i) Through a change in ring gain, one can tune the dimension in a wide range from 2 to 8. (ii) There are two different regimes, one for $G \approx 1.1$–1.7 dB and the other for $G \approx 1.7$–2.5 dB. Since the second ring eigenmode was excited at $G \approx 1.7$ dB, as shown in Fig. 3, one can easily see that the first regime corresponds to the situation where only one ring eigenmode was excited in the ring, and the second regime corresponds to the two-eigenmode situation. (iii) In both regimes, the dimension increases roughly linearly with gain, but the rate of the dimension change with gain is greater in the second regime. (iv) When one moves from the first regime to the second, there is a sharp jump in correlation dimension of about 1.

Figure 6 shows the autocorrelation function (ACF) data obtained with the following equation:

$$\mathrm{ACF}(\tau) = \frac{\sum_i [V(t_i) - \bar{V}][V(t_i + \tau) - \bar{V}]}{\sum_i [V(t_i) - \bar{V}]^2}, \qquad (3)$$

where $\bar{V}$ is the mean value of $V(t_i)$ and τ is the delay time. Graph (a) show the ACF vs. delay time profiles for signals obtained at different ring gains. Graph (b) shows the same data in a longer time scale. In both graphs, the vertical axes give the ring gain, and "red" and "dark blue" represent maximum and minimum ACF values, respectively. Graph (c) shows the full width at half maximum (FWHM) of the main ACF peak at $\tau = 0$ as a function of gain. The FWHM values were determined in different ways for the ACF profiles in the two regimes. In the one-eigenmode regime, the FWHM was determined simply by finding the time where the ACF profile first crossed 0.5. In the two-eigenmode regime, the FWHM value was determined by fitting a parabola to the section of the ACF profile between $\tau = 0$ μs and $\tau = 0.3$ μs and finding the point at which this parabola crossed half its value at $\tau = 0$ μs. Graphs (d) and (e) show the positions and amplitudes, respectively, of the first and second side ACF peaks as a function of gain.

Several results are evident in Fig. 6. (i) The data show two regimes, a one-eigenmode regime and a two-eigenmode regime, just as the correlation data showed in Fig. 5(d). (ii) When one moves from the first regime to the second, fast oscillations appear on the main peak, as shown in graph (a). Indeed, such oscillations are also on the side peaks, but this is not shown clearly in graph (b). This oscillation response corresponds to the appearance of the fast oscillations shown in Fig. 4(d). (iii) With an increase in gain, the main peak becomes narrower, as shown in graphs (a) and (c). (iv) The side peaks move toward the main peak as one increases the gain, as shown in graphs (b) and (d). This change is more pronounced in the transition but is less pronounced in the two-eigenmode

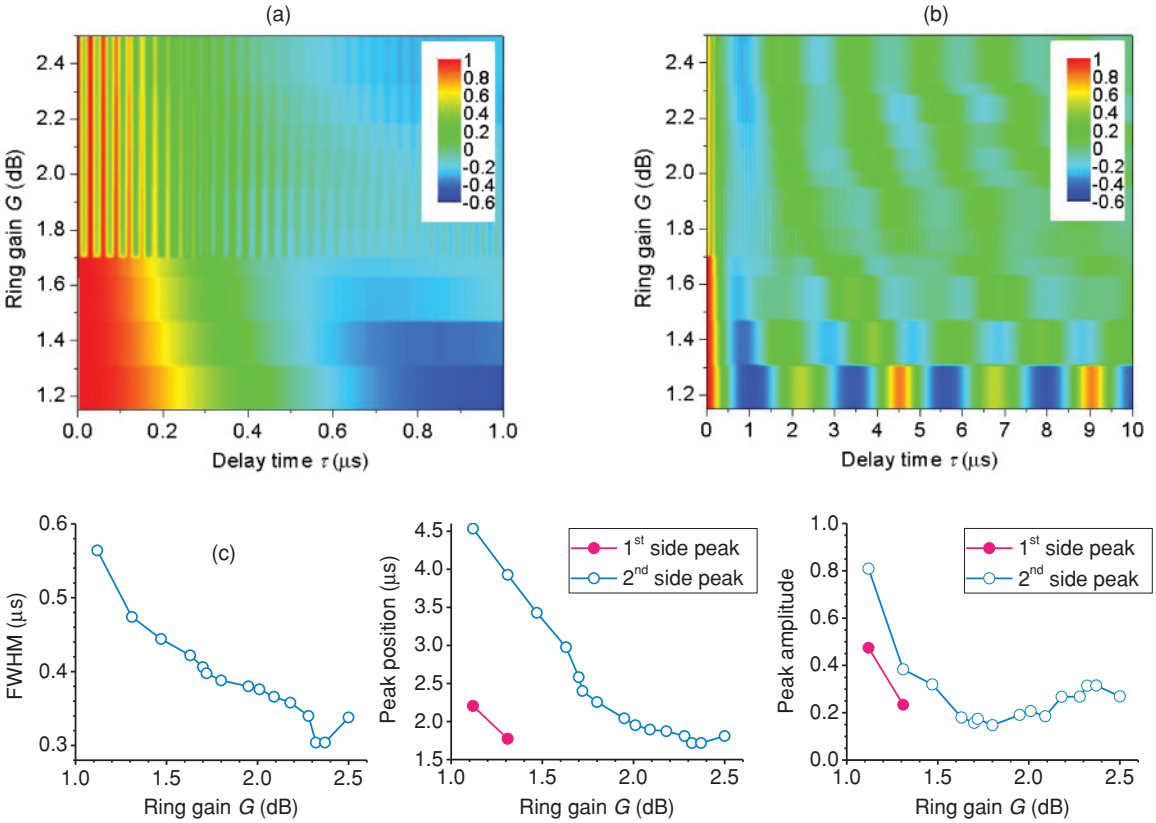

FIG. 6. (Color online) Graph (a) shows the autocorrelation function (ACF) profiles for signals obtained at different ring gains. Graph (b) shows the same data in a longer time scale. Graph (c) shows the full width at half maximum (FWHM) of the main peak as a function of gain. Graphs (c) and (d) show the positions and amplitudes, respectively, for the first and second ACF side peaks as a function of gain.

regime. (v) In the one-eigenmode regime, the amplitudes of the side peaks decrease with gain, as shown in graph (e). In the two-eigenmode regime, however, the amplitudes increase slightly with gain. These results demonstrate that one can easily tune the ACF properties through the ring gain. Note that the ACF properties of chaotic signals are important from a practical point of view. High-resolution chaotic radars, for example, demand chaotic signals with very sharp main ACF peaks and very weak side ACF peaks.

IV. SUMMARY

The data presented above clearly show that there are rich layers of complexity in chaotic spin waves in magnetic-film feedback rings. The results have important implications on chaotic dynamics in other feedback ring systems, such as electromagnetic transmission line oscillators and fiber ring lasers. In particular, one can expect similar behavior in feedback systems where sideband modes can be excited near the ring eigenmodes. The data also show that the complexity of the chaotic spin waves can be tuned easily by the ring gain. This easy tuning of the chaos complexity is of critical importance for radar applications. The radar for complex target detection, for example, relies on the tuning of features of chaotic signals to maximize the cross correlation of a transmitted signal with the reflection from one target and minimize the cross correlation of the transmitted signal with the reflection from another target.[23,24] Future study on the controlled tuning of chaos complexity in feedback rings through other parameters is of both fundamental and practical interest. Future work on the theoretical interpretation of the presented results is also of great interest. Several previous works have made use of the complex Ginzburg-Landau equation (CGLE) to explain the chaotic behavior in nonlinear optical rings.[10,11] This CGLE model, however, does not take into account the three-wave nonlinear processes that are responsible for the chaotic excitations in this work.

ACKNOWLEDGMENTS

This work was supported in part by the US National Science Foundation, the US Army Research Office, and the Russian Foundation for Basic Research.

*Corresponding author: mwu@lamar.colostate.edu

[1] D. S. Ricketts, X. Li, and D. Ham, IEEE Trans. Microwave Theory Tech. **54**, 373 (2006).
[2] D. Ham, X. Li, and D. S. Ricketts, IEEE Commun. Mag. **44**, 126 (2006).
[3] D. S. Ricketts, X. Li, N. Sun, K. Woo, and D. Ham, IEEE J. Solid-State Circuits **42**, 1657 (2007).
[4] V. E. Demidov and N. G. Kovshikov, Tech. Phys. Lett. **24**, 274 (1998).
[5] S. O. Demokritov, A. A. Serga, V. E. Demidov, B. Hillebrands, M. P. Kostylev, and B. A. Kalinikos, Nature (London) **426**, 159 (2003).
[6] M. Wu, B. A. Kalinikos, and C. E. Patton, Phys. Rev. Lett. **95**, 237202 (2005).
[7] M. Wu, B. A. Kalinikos, L. D. Carr, and C. E. Patton, Phys. Rev. Lett. **96**, 187202 (2006).
[8] L. Luo, T. J. Tee, and P. L. Chu, J. Opt. Soc. Am. B **15**, 972 (1998).
[9] H. D. I. Abarbanel, M. B. Kennel, M. Buhl, and C. T. Lewis, Phys. Rev. E **60**, 2360 (1999).
[10] J. M. Soto-Crespo and N. Akhmediev, Phys. Rev. E **70**, 066612 (2004).
[11] L. M. Zhao, D. Y. Tang, and A. Q. Liu, Chaos **16**, 013128 (2006).
[12] A. K. Komarov, Opt. Spectrosc. (USSR) **102**, 637 (2007).
[13] M. J. Ablowitz and H. Segur, *Solitons and the Inverse Scattering Transform* (SIAM, Philadelphia, 1985).
[14] N. Akhmediev and A. Ankiewicz, *Dissipative Solitons* (Springer, Berlin, 2005).
[15] N. Akhmediev, J. M. Soto-Crespo, and G. Town, Phys. Rev. E **63**, 056602 (2001).
[16] V. E. Demidov and N. G. Kovshikov, JETP Lett. **66**, 261 (1997).
[17] V. E. Demidov and N. G. Kovshikov, Tech. Phys. Lett. **24**, 647 (1998).
[18] A. V. Kondrashov, A. B. Ustinov, B. A. Kalinikos, and H. Benner, Tech. Phys. Lett. **34**, 492 (2008).
[19] A. M. Hagerstrom, W. Tong, M. Wu, B. A. Kalinikos, and R. Eykholt, Phys. Rev. Lett. **102**, 207202 (2009).
[20] M. Wu, A. M. Hagerstrom, R. Eykholt, A. Kondrashov, and B. A. Kalinikos, Phys. Rev. Lett. **102**, 237203 (2009).
[21] Z. Liu, X. Zhu, W. Hu, and F. Jiang, Int. J. Bifurcation Chaos **17**, 1735 (2007).
[22] V. Venkatasubramanian and H. Leung, IEEE Signal Process. Lett. **12**, 528 (2005).
[23] T. L. Carroll, Chaos **17**, 033103 (2007).
[24] T. L. Carroll, IET Radar Sonar Navig. **2**, 256 (2008).
[25] A. S. Dmitriev, B. E. Kyarginskii, A. I. Panas, D. Yu. Puzikov, and S. O. Starkov, Tech. Phys. Lett. **29**, 72 (2003).
[26] M. Chen, M. A. Tsankov, J. M. Nash, and C. E. Patton, Phys. Rev. Lett. **70**, 1707 (1993).
[27] D. D. Stancil and A. Prabhakar, *Spin Waves—Theory and Applications* (Springer, New York, 2009).
[28] A. G. Gurevich and G. A. Melkov, *Magnetization Oscillations and Waves* (CRC, Boca Raton, 1996).
[29] P. S. Addison, *Fractals and Chaos* (Institute of Physics, Bristol, 1997).
[30] F. M. de Aguiar, A. Azevedo, and S. M. Rezende, Phys. Rev. B **39**, 9448 (1989).
[31] H. S. Kim, R. Eykholt, and J. D. Salas, Physica D **127**, 48 (1999).